Monitoring Systemic Dynamic Effects following Disturbances affecting HVDC Power Transmission in the BIPS using WAMS Infrastructure

Daniel S. da Silva*†, Guido R. Moraes*†, Leandro D. Penna‡, Ildemar C. Decker*†,
Antonio F. C. Aquino*†, Diego Issicaba*†
*Federal University of Santa Catarina, Florianópolis, Brazil
†INESC P&D Brasil, Santos, Brazil
‡Operador Nacional do Sistema Elétrico, Rio de Janeiro, Brazil

***Abstract*—This paper introduces a conceptual framework and infrastructure designed to monitor the dynamic behavior of the Brazilian Interconnected Power System (BIPS) following disturbances that affect power transmission in High Voltage Direct Current (HVDC) links. Monitoring is devised in light of a set of proposed System Severity Indicators (SSIs), whose computation depends upon synchrophasor data collected at converter stations and conveyed to a phasor data concentrator (PDC) placed in the control center of the Brazilian System Operator (BSO). Numerical results are acquired using electromagnetic transient (EMT) simulation and actual disturbance records, including cases with commutation failures and DC transmission line fault events. The results highlight the applicability of the proposed indicators on featuring the severity of events to the transient stability of the BIPS.**

***Index Terms*—WAMS, HVDC, Brazilian Interconnected Power System, Multi-infeed operation.**

I. Introduction

In multi-infeed HVDC large power grids, the dynamic performance may be severely affected by sudden variations in the HVDC power transmission. Commutation failures caused by short-circuits in the AC grid and faults on DC transmission lines are among the most common causes of DC power transmission disturbances. Particularly, in power systems with embedded DC links, HVDC forced outages and commutation failures following critical AC transmission contingencies may deteriorate the rotor angle stability, increasing the risks of out-of-step generators and cascading outages. These characteristics can be found in the BIPS, composed of six HVDC bipoles in multi-infeed configuration, two of them embedded in the main AC grid [1].

In the literature, there are numerous WAMS applications focused on the monitoring of systemic events in AC grids, taking advantage of the synchronicity provided by Phasor Measurement Units (PMUs) in the assessment of the dynamic behavior of power systems under perturbations. As in recent instances, methodologies based on frequency measurements have been proposed for automatic post-event analysis in [2], [3], [4], while advances in rotor angle stability monitoring, with concerns on the impacts of systemic events, can be found using model-dependent [5] or model-free approaches [6], [7]. On the other hand, regarding the assessment of the impacts on the power system dynamics resulting from multi-infeed and embedded HVDC transmission events, there is a lack of works that exploit the benefits of applying synchronized measurements in monitoring these special system configurations. Regarding disturbances in DC power transmission, synchrophasor-based approaches are usually devoted to CF detection [8] and mitigation [9]. In [10], an analytical examination of the impacts of a CF is presented. In [11], a CF immunity index is proposed, which consists of a parameter-based formula to assess the CF susceptibility of a system, while the effects of local and concurrent CFs are analyzed through simulations. Concurrent CFs analysis is also proposed in [12], through the calculation of an interaction factor and the simulation results.

In this context, this paper proposes a conceptual framework based on a WAMS infrastructure designed to monitor the dynamic performance of the BIPS after disturbances that affect the power transmission of the HVDC links. At the best of authors' knowledge, this is the first synchrophasor-based approach, in the state of the art, focused on the problem of monitoring the systemic impact following disturbances that affect HVDC links. The specification of the conceptual framework and infrastructure covers the converter stations of the six HVDC links of the BIPS, encompassing the development of customized SSIs, aiming at exploiting synchrophasor data to characterize the severity of disturbances to the power system dynamics. The calculation and processing of SSIs is also envisioned to allow enhancements in the modelling of events affecting HVDC power transmission in power system studies, enabling increased accuracy in determining transmission capacity limits among areas of the BIPS.

The designed SSIs take into account the power recovery time (RT) and the energy not transmitted (ENT) for all HVDC links, as well as the maximum swing of the phase angle difference ($\Delta\theta$) between the phasor voltages at the embedded HVDC converter stations. The first two indicators are defined on the basis of power signals, with a focus on events with sudden variation of power exchange between AC and DC systems. The indicator $\Delta\theta$ allows monitoring the severity of events from the point of view of maximum rotor angle excursions, which is a relevant measure

of the dynamic behavior of AC systems. Indicators are computed following a moving window, whereas non-neglectful alterations in HVDC power transmission at monitored bipoles are identified through the application of a straightforward Teager-Kaiser energy-based procedure.

Numerical results are acquired using EMT simulation and actual disturbance records, involving cases with commutation failures and DC transmission line fault events. Case studies include the simulation of faults at 345 and 500 kV substations of the BIPS, resulting in commutation failure in one or more converter stations, as well as faults in the DC transmission lines with successful and unsuccessful restart sequences. Simulations have been performed with a dynamic equivalent system of the BIPS [13] built in PSCAD/EMTDC and provided by the BSO. The results show that the proposed approach is sufficiently generic to be adopted by System Operators of large AC/DC power systems, highlighting the relevance of employing the proposed monitoring to reduce uncertainties in the definition of power flow limits.

The paper is organized as follows. Section II introduces the proposed conceptual framework of application. Section III presents the mathematical expressions applied to the evaluation of the severity of disturbances that affect HVDC power transmission. Section IV shows numerical results, while final remarks are presented in Section V.

II. Proposed Framework of Application

The BIPS is supported by a diversified electricity matrix, characterized by a powerful set of hydroelectric power plants and an increasing share of wind and solar power plants. Regarding the transmission system, the HVAC and HVDC interconnections play an important role, allowing the transfer of electrical energy between the Brazilian regions. The BIPS benefits from the inherent complementary availability of energy resources throughout the country, which spans a continent-sized territory. Moreover, the BIPS includes six HVDC bipoles: Xingu-Estreito (BXE) and Xingu-Terminal Rio (BTR), both with 4.000 MW capacity, $\pm$ 800 kV; Coletora Porto Velho-Araraquara 1 and 2 (BMC1 & BMC2) and Foz do Iguaçu-Ibiúna 1 and 2 (BI1 & BI2), the four bipoles with 3.150 MW capacity, $\pm$ 600 kV. It should be noted that BXE and BTR constitute embedded HVDC links, which connect the Belo Monte hydroelectric power plant to the main load center of the BIPS, in the southeast of Brazil.

Forced outages or commutation failures in the HVDC links, especially those embedded, can severely deteriorate the rotor angle stability of the power system. This raises concerns to the BSO on how to monitor these events and their repercussions in the dynamic behavior of the BIPS. In Fig. 1, it is presented the conceptual framework devised to monitor systemic dynamic effects after disturbances that affect the power injection of HVDC links, which together represent 20.6 GW of installed capacity. It relies on the installation of PMUs placed at all converter stations, using a dedicated Wide Area Monitoring System (WAMS), deemed to enhance the BSO capacity to monitor the dynamic performance of

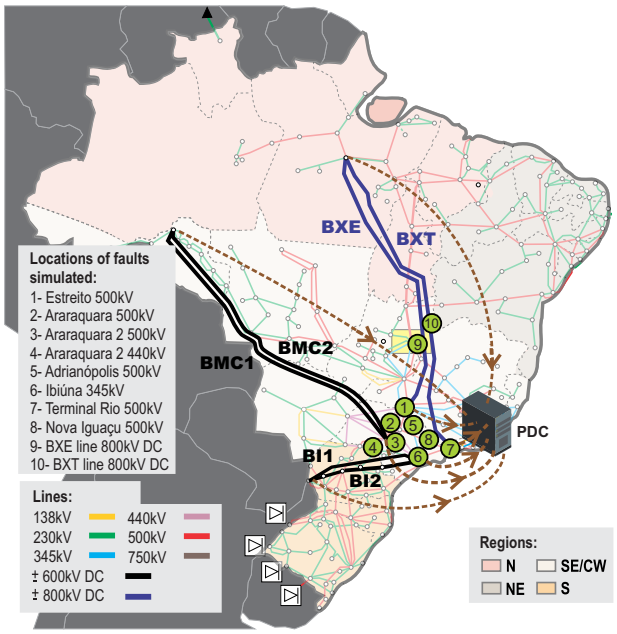

Fig. 1. Conceptual framework of application.

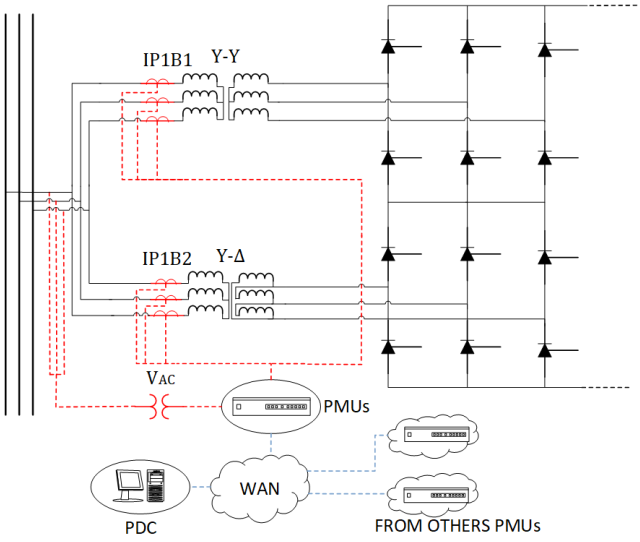

Fig. 2. Specified infrastructure for each HVDC pole (two-winding transformers).

the BIPS during large disturbances. Based on synchronized data from converter stations located up to 2,500 km apart, SSIs related to each disturbance can be calculated and analyzed, providing valuable information for the system operation.

The specified infrastructure for each HVDC pole with 2-winding transformers is shown in Fig. 2. Three-phase current measurements are acquired at the HV terminals of the Y-Y and Y-Δ converter transformers. Additionally, three-phase voltage measurements are acquired at the bay of each converter transformer. In compliance to the IEEE C37.118.2-2011 protocol [14], the measurements are processed by the PMUs and transmitted at a rate of 120 frames per second to PDCs placed at the converter

stations, where the data can be stored in case of communication channel unavailability. Using the STTP protocol, PDCs placed at the converter stations send synchronised data to a PDC located at a control center, where visualization tools are made available. Within the PDC servers, Grid Protection Alliance (GPA) open-source software components known as Open Phasor Data Concentrator (openPDC) and openHistorian 2 are executed.

III. Evaluation of Severity of Systemic Disturbances

The developed SSIs are associated with the amount of interrupted power in the HVDC links and the dynamic recovery of the power injection. Active power signals are obtained from voltage and current signals acquired from the dedicated WAMS, and the computation of SSIs is triggered by a detection procedure based on the application of the Teager-Kaiser Energy Operator ($TKEO$). The $TKEO$ is a useful tool for the analysis of the energy of a signal, widely applied in signal [15], [16] and image processing [17], [18], as well as in the detection, classification and location of power system events [19]. The discrete $TKEO$ can be defined by the expression

$$\lambda(x[n]) = x^2[n] - x[n-1]x[n+1] \tag{1}$$

where x represents the signal and n is an index for the signal sample.

Eq. (1) is applied to the active power signal obtained through a continuous moving window. If the $TKEO$ overpasses a threshold Th_{TKEO}, adjusted using real-time operation data, the occurrence of an event is characterized. After the detection of an event, a pre-defined amount of active power samples is stored for the calculation of the designed SSIs, namely, the recovery time (RT), the total energy not transmitted (ENT) and the variation of phase angle difference ($\Delta\theta$).

The RT is the recovery time of 90% of the total power P_{o}, immediately before the event, transmitted through the HVDC links. The reference value of $90\%P_{\text{o}}$ is also adopted by the BSO in the grid requirements applied to each DC link. Power transmission after a commutation failure is usually recovered with a significant slope until it reaches approximately 90% of its original value before failure, when recovery slows down, due to the adopted HVDC control. Linear interpolation is employed to obtain $90\%P_{\text{o}}$, and the RT is calculated according to the expressions

$$T_{\text{ini}} = t[n-1],\ if\ P[n] < 0.9P_{\text{o}} \tag{2}$$

$$T_{\text{end}} = t[n],\ if\ P[n] \geq 0.9P_{\text{o}} \tag{3}$$

$$RT = T_{\text{end}} - T_{\text{ini}} \tag{4}$$

where $t[n]$ is the time instant of sample n; P denotes the sum of the active power monitored from the HVDC links; P_{o} denotes the steady-state pre-fault operation value of the summed active power from HVDC links; T_{ini} and T_{end} are initial and final instants used to calculate RT, respectively. Once an interruption of power transmission occurs, as well as (2) and (3) are satisfied, RT is computed using (4).

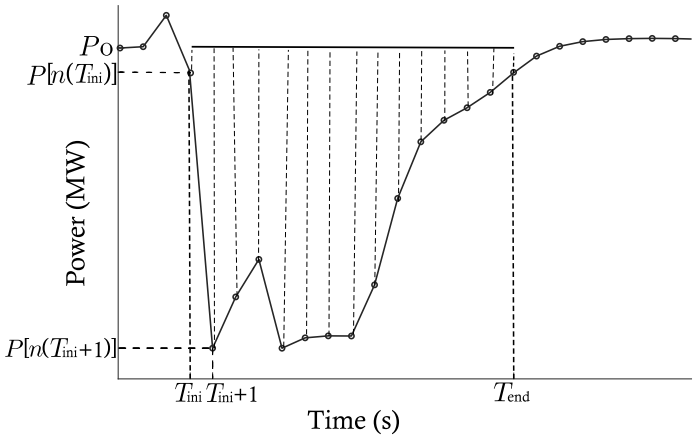

Fig. 3. Example of ENT areas.

The ENT (in $MW.s$) takes into account the power interrupted and its duration, and is calculated in terms of T_{ini} and T_{end}, as shown in Fig. 3. The ENT corresponds to the contained area between P_{o} and $P[n]$, in between T_{ini} and T_{end}. This area can be divided into smaller areas every two samples, and such smaller areas are approximated through the expressions of rectangular trapezoids. Let n_{ini} and n_{end} be the samples corresponding to T_{ini} and T_{end}, respectively, ENT can be computed according to the expression

$$\begin{aligned} ENT = & \frac{((P_{\text{o}} - P[n_{\text{ini}}+1]) + (P_{\text{o}} - P[n_{\text{ini}}]))\,(T_{\text{ini+1}} - T_{\text{ini}})}{2} \\ & + \frac{1}{f}\sum_{j=n_{\text{ini}}+1}^{n_{\text{end}}-2} \frac{(P_{\text{o}} - P[j+1]) + (P_{\text{o}} - P[j])}{2} \\ & + \frac{((P_{\text{o}} - P[n_{\text{ini}}-1]) + (P_{\text{o}} - P[n_{\text{end}}]))\,(T_{\text{end}} - T_{\text{end-1}})}{2} \end{aligned} \tag{5}$$

The variation of phase angle difference between the North and Southwest subsystems, denoted as $\Delta\theta$, represents the maximum variation in voltage angle between the rectifier terminal and inverter terminal of the HVDC link. The indicator $\Delta\theta$ is defined as

$$\Delta\theta = max(\theta_{\text{post-fault}}) - \theta_{\text{pre-fault}} \tag{6}$$

where θ is the difference between the phase angle signals acquired at the rectifier and the inverter terminals, $\theta_{\text{post-fault}}$ denotes the maximum value following a disturbance (neglecting abrupt variations/spikes caused by short-circuits), and $\theta_{\text{pre-fault}}$ is the steady-state value pre-perturbation. In the context of the BIPS, θ is evaluated for the the two HVDC links that connect north to south, denoted θ_{BXE} and θ_{BXT}, for the HVDC links of BXE and BXT, respectively. Since these two HVDC links are embedded in the AC grid, θ_{BXE} and θ_{BXT} are directly associated with the angles of the rotors of the generating machines of these regions of the BIPS.

The summary of the procedure that involves acquiring the data, processing (detection step) and calculating the SSIs (SSI

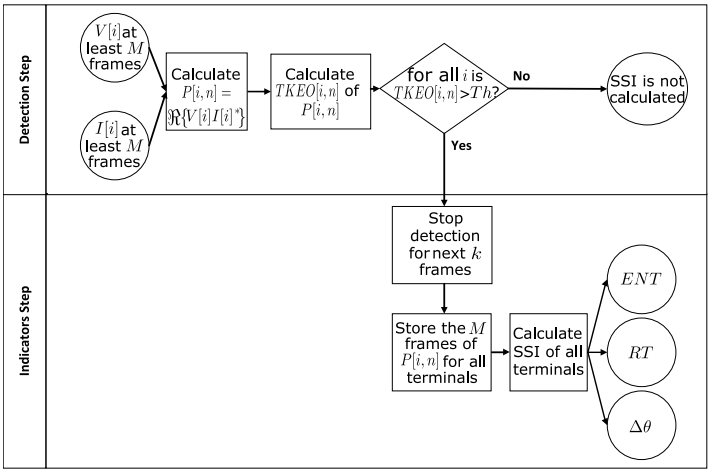

Fig. 4. Evaluation procedure of severty indicators.

calculation step) can be seen in Fig. 4. The input signals are the voltages V_{AC} and currents I_{AC} on the high voltage (HV) side of the converter transformers, evaluated at each sample n and terminal i, respectively. The $TKEO[i,n]$ is calculated using (1). If the resulted $TKEO[i,n]$ overpass the threshold Th, an event is detected. The detection is then disabled for the next k frames to avoid false positive detections and the SSIs are calculated for all terminals i. The parameters M and k are specified as 600 and 18 samples, respectively.

IV. Numerical results and discussions

This section is divided into four subsections. In Subsection IV-A, a description of the simulation cases is provided. In Subsection IV-B, results for a first case are detailed to illustrate the application of the designed algorithms. In Subsection IV-C, results for multiple simulation cases are summarized. In Subsection IV-D, a real case of commutation failure in the BIPS is addressed with the proposed approach.

A. Description of the simulation cases

Simulation cases have been meticulously chosen to encompass a variety of event types within both the HVDC link and AC grid. The primary objective is to identify potential power interruption events capable of impacting the dynamic behavior of BIPS.

The simulations have been performed in PSCAD/EMTDC with an equivalent BIPS system (as detailed in [20]). These simulations take into account the following scenarios: (i) maximum power transfer for bipoles BXE and BXT at 2 x 4,000 MW; (ii) bipoles BMC1 and BMC2 with a combined power of 6,000 MW; (iii) bipoles of BI with a collective power of 4,200 MW; (iv) HVDC models provided by the respective manufacturers; (v) simulation models comprising dynamic and static equivalents, incorporating a detailed representation of significant power plants relevant to the involved phenomena (e.g. hydroelectric plants named Belo Monte, Tucuruí, Estreito, Furnas, Angra 2); and (vi) an equivalent representation of the AC North-Southeast interconnection, established via two 500 kV transfer equivalents connecting frontier buses and the modeled subsystems.

Simulations have been performed assuming 100 ms single-phase solid short-circuits at substations and at the DC transmission lines, as can be seen in Fig. 1. In cases 1 to 8, due to the short-circuits simulated in the substations, CF events occurred in some of the BIPS bipoles. In cases 9 to 10, the short-circuits have been simulated at the BXE HVDC-LCC link. Unsuccessful restart in cases of DC fault simulations are enforced by the protection system of the HVDC system, 150ms after the start of the event. The simulation records have 5 seconds of duration and were provided by the BSO in the Common format for Transient Data Exchange for power systems (COMTRADE).

As a general reference of the impacts caused by the short circuits simulated, Table I presents the Time Duration of Interrupted Power Transfer (TDIPT), in ms, for every simulation case (lines of the table) and for every bipole (columns 3 to 7). Bipoles BI1 and BI2 are accounted together in column 7. In column 8 is presented the total TDIPT for each case. The TDIPT is calculated based on the simulation data recorded at the AC terminals of each bipole. As an example, in Case 1, the simulated short circuit in the Estreito 500 kV substation leads to CFs in BCM1, BCM2 and BI bipoles and associated TDIPTs assume non-zero values.

TABLE I
TDIPT (MS) IN THE SIMULATION CASES

Case	Fault location	BCM1	BCM2	BXE	BXT	BI	Total
1	Estreito 500 kV	5	59	105	-	30	199
2	Araraquara 500 kV	111	103	77	14	45	350
3	Araraquara 2 500 kV	121	125	100	8	44	398
4	Araraquara 2 440 kV	107	99	85	14	99	349
5	Adrianópolis 500 kV	6	68	75	148	38	335
6	Ibiúna 345 kV	6	76	86	6	130	304
7	Terminal Rio 500 kV	149	5	9	75	44	282
8	Nova Iguaçu 500 kV	147	1	1	66	45	360
9	BXE line 800 kVcc	-	-	150	-	-	150
10	BXT line 800 kVcc	-	-	12	150	-	162

In order to produce phasors from oscillographies in COMTRADE format, a PMU simulator has been developed based on [21] and implemented in MATLAB with all recommendations defined in [22]. PMUs have been modeled as class M, with reporting rate of 60 fps. Events are detected using the threshold Th_{TKEO} of 0.36 pu^2.

B. Simulation results for Case 1

In Case 1, the short-circuit simulated at Estreito 500 kV substation leads to a CF of medium severity in BXE and BMC2, CF of low severity in BMC1, and absence of CF in BXT, taking into consideration the TDIPTs in Table I.

The results of the processing and detection step can be seen in Fig. 5. Figure 5(a) shows the active power transmitted, calculated at the Y-Y converter transformer of the inverter terminals. Note the significant sag in all signals, except for the BXT (blue). In Fig. 5(b), the results of the application of the $TKEO$ are presented, and the threshold (red horizontal line) is initially overpassed by

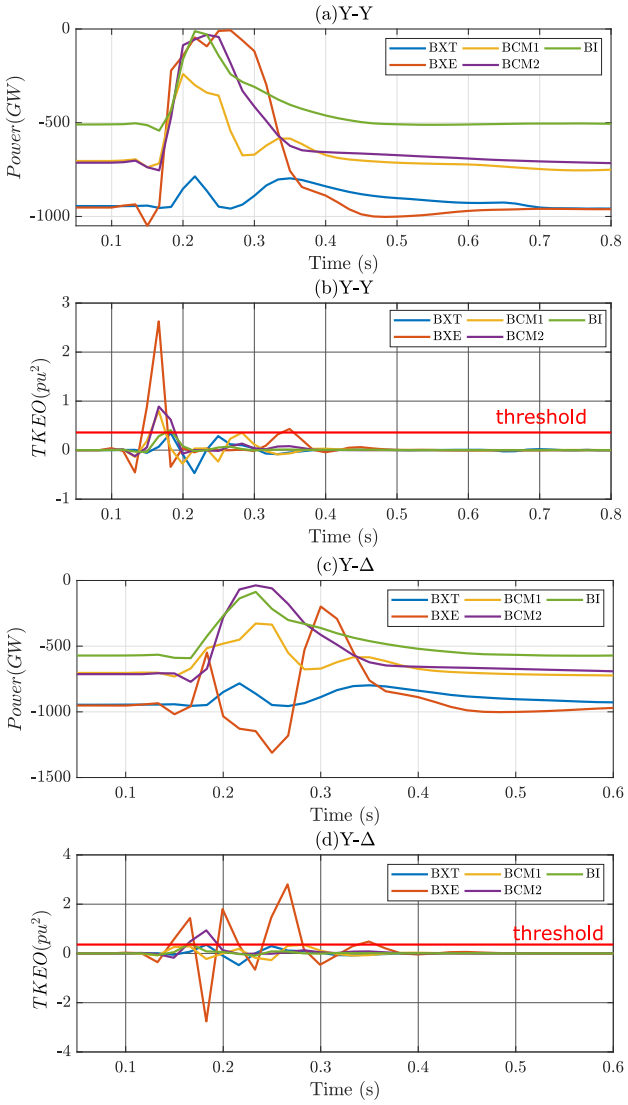

Fig. 5. Active power calculated and $TKEO$ results for Case 1.

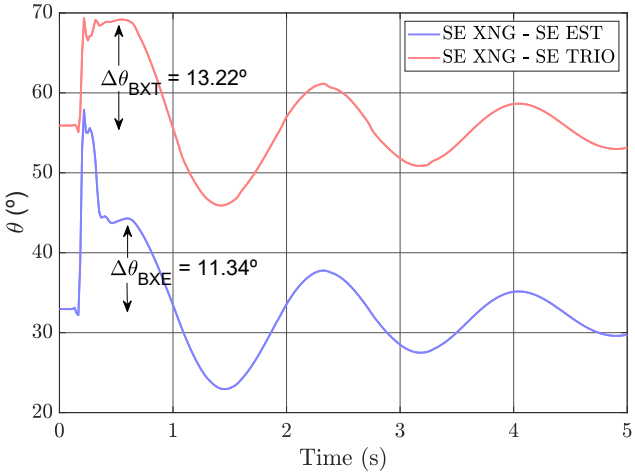

Fig. 6. Phase angle difference in case 1.

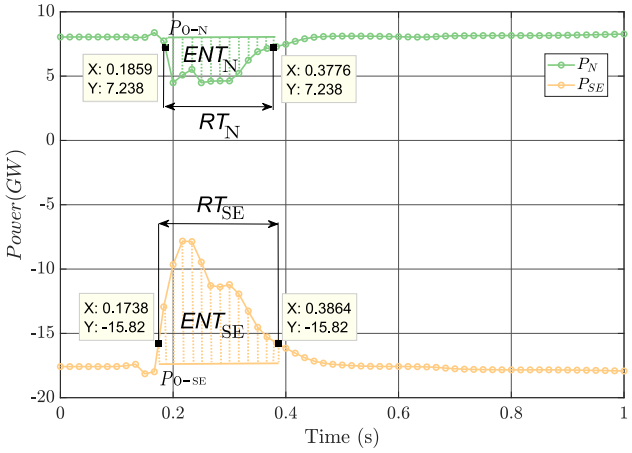

Fig. 7. ENT calculation in Case 1

BXE, BCM1, BCM2, and BI, and later by BXT. The active power transmitted and the $TKEO$ application results of the Y-Δ converter transformers can be seen in Fig. 5(c) and Fig. 5(d), respectively.

The $\Delta\theta_{\text{BXE}}$ and $\Delta\theta_{\text{BXT}}$ are depicted in Fig. 6. The phase angle difference of BXE is shown in blue, calculated by the difference in synchrophasor voltage angles between SE Xingu 500 kV and SE Estreito 500 kV. Similarly, the phase angle difference of BXT is shown in red, calculated using the synchrophasor voltage angles between SE Xingu 500 kV and SE Terminal Rio 500 kV. The colored black arrows represent $\Delta\theta_{\text{BXE}}$ and $\Delta\theta_{\text{BXT}}$. The calculated values for $\Delta\theta_{\text{BXE}}$ and $\Delta\theta_{\text{BXT}}$ are 11.34° and 13.22°, respectively. The value used to calculate $\Delta\theta$ is the maximum angle observed after the initial transient, allowing the capture of the phenomenon of interest, associated with the rotor oscillations of the generating units, following the event. The initial spike is attributed to electrical effects in the synchrophasors registered, in this case, related to the impacts of the short-circuit and the commutation failures.

In Fig. 7, the sum of the transferred power at the HVDC links associated with BXE and BXT is represented by the green line, while the sum of the transferred power at the HVDC links associated with the inverter terminal of the Southeast region (BXE, BXT, BCM1, BCM2 and BI) is denoted by a yellow line. The black dots with the coordinates X and Y were interpolated, representing $0.9P_0$ in Y as well as T_{ini} and T_{end} in X. The areas used to calculate ENT_{N} and ENT_{SE} are indicated by dashed lines in green and yellow, respectively, for north and southeast regions. The indicators ENT_{N} and ENT_{SE} correspond to 465 MWs and -1212 MWs, respectively, while the indicators RT_{N} and RT_{SE} correspond to 191 ms and 212 ms, respectively.

C. Summary of results of all simulation cases

The results of the developed SSIs calculated for all simulation cases are presented in Table II. First, it can be seen that the cases with less CFs (Cases 9, 10 and 1, in order), resulted in some of

the lowest $\Delta\theta_{\text{BXE}}$, $\Delta\theta_{\text{BXT}}$ and ENT_{SE} obtained. Notice that, for Case 1, $\Delta\theta_{\text{BXE}}$ is low even with the short circuit occurring in a location nearby the terminal of BXE, suggesting that $\Delta\theta_{\text{BXE}}$ is not strongly influenced by the location of the perturbation. The highest values of $\Delta\theta_{\text{BXE}}$ and $\Delta\theta_{\text{BXT}}$ occur in cases V and VII, in which the fault occurred nearby the inverter terminal of BXT. In contrast to Case 1, all the terminals analyzed suffered CF in Cases 5 and 7, corroborating with the hypothesis that $\Delta\theta_{\text{BXE}}$ and $\Delta\theta_{\text{BXT}}$ are indicators of interest to the severity of the events under analysis. Notice that ENT_{N} also presents adherence to $\Delta\theta_{\text{BXE}}$ and $\Delta\theta_{\text{BXT}}$, in terms of general ascending sort of results, for cases 1 to 8. On the other hand, in cases 9 and 10, the short circuits in BXE and BXT lines directly influenced the indicators.

TABLE II
SSIs RESULTS FOR THE SIMULATION CASES

Case	Fault location	$\Delta\theta_{\text{BXE}}$ (°)	$\Delta\theta_{\text{BXT}}$ (°)	ENT_{N} $(MW.s)$	ENT_{SE} $(MW.s)$
1	Estreito 500 kV	11.34	13.22	+476	-1223
2	Araraquara 500 kV	15.13	18.81	+687	-1886
3	Araraquara 2 500 kV	15.41	19.18	+674	-1899
4	Araraquara 2 440 kV	14.86	18.32	+680	-1840
5	Adrianópolis 500 kV	16.51	20.09	+898	-1610
6	Ibiúna 345 kV	14.40	17.96	+656	-1763
7	Terminal Rio 500 kV	16.36	19.63	+893	-1602
8	Nova Iguaçu 500 kV	16.12	18.73	+806	-1560
9	BXE line 800 kVcc	8.33	9.53	+852	-860
10	BXT line 800 kVcc	14.14	15.13	+1022	-1030

The relationship between $\Delta\theta_{\text{BXE}}$, $\Delta\theta_{\text{BXT}}$, ENT_{N}, and CFs may be better verified in Fig. 8. In the figure, ENT_{N} was selected instead of ENT_{SE} because it is directly associated with the voltage angle of the rectifier terminal, which is used to calculate $\Delta\theta_{\text{BXT}}$. In the legend, BCF denotes Bridges under Commutation Failure, evaluated through the simulations, and verified through visual assessment of oscillographies. In Fig. 8, the coordinates X and Y represent ENT_{N} and $\Delta\theta_{\text{BXE}}$ (subfigure a), ENT_{N} and $\Delta\theta_{\text{BXT}}$ (subfigure b).

In particular, the cases where the BCF has been equal to 9 or 10 presented a similar behavior, with high $\Delta\theta_{\text{BXE}}$ and $\Delta\theta_{\text{BXT}}$. Analyzing only $\Delta\theta_{\text{BXT}}$, the results in which the BCF is equal to 9 or 10 are even more distinct from the results with fewer BCFs. As previously reported, disconsidering Cases 9 and 10, the results with BCF=9 and BCF=10 also present the highest ENT_{N}.

D. Results for a real case

The real case selected is a CF event that occurred in the BMC2 bipole on 01/16/2020, at 22h21min21s (UTC-3), and lasted 56 ms. The oscillographic data (acquired at 15.36 kHz sampling rate) have been used to confirm the occurrence of the CF. The synchrophasor data, provided by the BSO, have been acquired by PMUs installed at poles 1 and 2 of BMC2. The event was initiated by an AC short circuit caused by vegetation interference in the transmission system near the Araraquara 2 500 kV substation, the inverter terminal of BMC2. The actual data set comprises data only from the BMC2 bipole, and it has been used

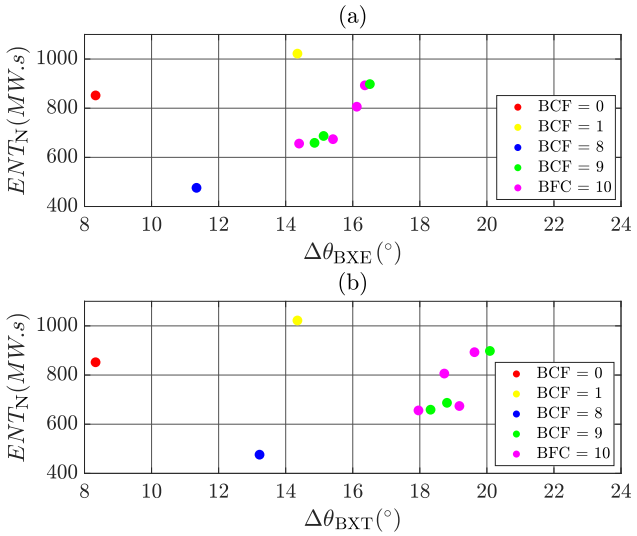

Fig. 8. ENT_{N} x $\Delta\theta$ for all simulations case.

to test the detection threshold and to calculate the energy not transmitted at BMC2 ENT_{BMC2}.

The active powers $P[n]$ recorded at pole 1 in converter transformers Y-Y (BYY1 in red line) and Y-D (BYD1 in brown square) and pole 2 in converter transformers Y-Y (BYY2 in yellow circle) and Y-D (BYD1 in purple line and asterisk marker) at the inverter terminal of BMC2 are presented in Fig. 9(a), based on phasor measurements. As expected, the active power of both bridges has abruptly decreased, reaching values of almost 100 MW. The $TKEO$ is calculated in Fig. 9(b), and has achieved a value higher than 0.4 pu in all signals, which represents more than the specified threshold, correctly indicating a disturbance that can affect power transmission in the BIPS. The SSIs ENT_{BMC2} (in orange dot line) and RT_{BMC2} of the bipole, at the inverter station, can been seen in Fig. 10. The value of ENT_{BMC2} and RT_{BMC2} are 213 $MW.s$ and 160 ms, respectively.

V. FINAL REMARKS

In this paper, a synchrophasor-based framework and infrastructure have been presented to monitor systemic dynamic effects after disturbances that affect the transmission of HVDC power. The framework is divided into an event detection step and SSI calculation step, where the proposed SSIs are calculated. The proposed SSIs evaluate the total energy not transmitted in bipoles following CFs and short circuits, the recovery time of power transmitted and the variation of phase angle difference between terminals, an indicator of synchronism. The infrastructure proposed was planned for the BIPS, a large and complex power system constituted by six bipoles in multi-infeed configuration, two of them embedded in the AC grid, which served as case study in simulations and in tests with real data. The results obtained with simulated data and real data show the robustness of the detection step, and analysis of the results obtained in the indicator step shows the benefits of adopting the proposed SSIs to identify severe cases, based on synchrophasor-based indicators.

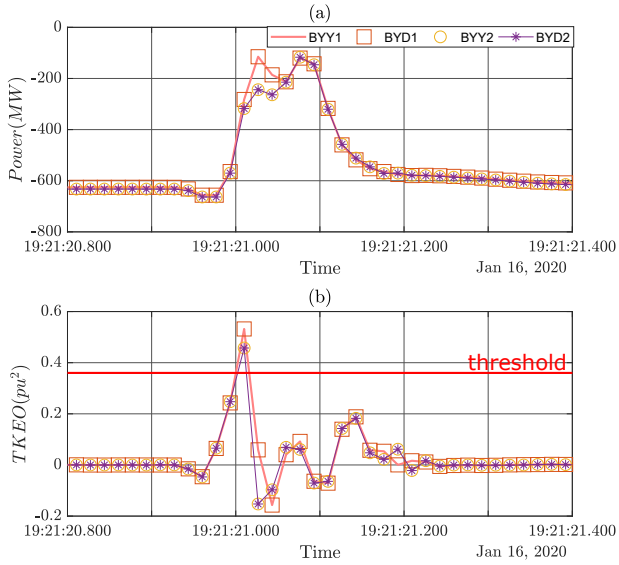

Fig. 9. Active power and TKEO results for a real case.

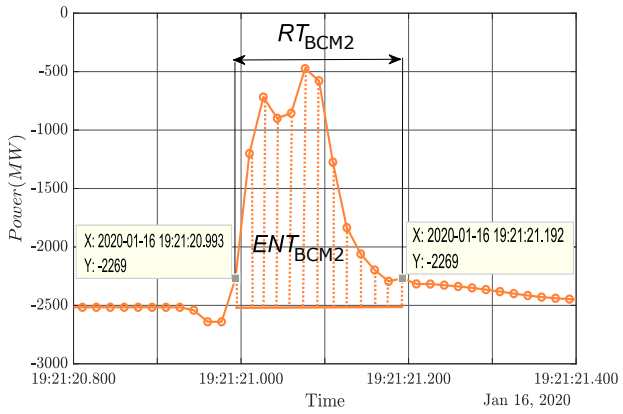

Fig. 10. ENT and TR for a real case.

Future works focus on the specification of the pilot project, considering PMU installations in all converter stations, as well as implantation of the SSI computation and visualization functions within the control center of the BSO.

Acknowledgement

This work has been supported by the BSO (project code OC-0001786-0).

References

[1] G. R. Moraes, B. A. Ambrósio, J. L. Pereira, D. Issicaba, A. F. Aquino, and I. C. Decker, "Impact analysis of COVID-19 pandemic on the electricity demand, frequency control and electromechanical oscillation modes of the Brazilian interconnected power system using low voltage wams data," *International Journal of Electrical Power & Energy Systems*, vol. 142, p. 108266, 2022.

[2] R. Vaz, G. R. Moraes, E. H. Arruda, J. C. Terceiro, A. F. Aquino, I. C. Decker, and D. Issicaba, "Event detection and classification through wavelet-based method in low voltage wide-area monitoring systems," *International Journal of Electrical Power & Energy Systems*, vol. 130, p. 106919, 2021. [Online]. Available: https://www.sciencedirect.com/science/article/pii/S0142061521001599

[3] G. Frigo, P. A. Pegoraro, and S. Toscani, "Tracking power system events with accuracy-based PMU adaptive reporting rate," *International Journal of Electrical Power & Energy Systems*, vol. 153, p. 109384, 2023. [Online]. Available: https://www.sciencedirect.com/science/article/pii/S0142061523004416

[4] Y. Kong, Y. Lu, and F. Tu, "Implementation of synchrophasor monitoring and event analysis at american electric power," in *2022 IEEE/PES Transmission and Distribution Conference and Exposition (T&D)*, 2022, pp. 1–5.

[5] J. Yan, C.-C. Liu, and U. Vaidya, "PMU-based monitoring of rotor angle dynamics," *IEEE Transactions on Power Systems*, vol. 26, no. 4, pp. 2125–2133, 2011.

[6] S. Dasgupta, M. Paramasivam, U. Vaidya, and V. Ajjarapu, "PMU-based model-free approach for real-time rotor angle monitoring," *IEEE Transactions on Power Systems*, vol. 30, no. 5, pp. 2818–2819, 2015.

[7] Y. Wu, M. Musavi, and P. Lerley, "Synchrophasor-based monitoring of critical generator buses for transient stability," *IEEE Transactions on Power Systems*, vol. 31, no. 1, pp. 287–295, 2016.

[8] H. Xiao, Y. Li, and X. Duan, "Enhanced commutation failure predictive detection method and control strategy in multi-infeed lcc-hvdc systems considering voltage harmonics," *IEEE Transactions on Power Systems*, vol. 36, no. 1, pp. 81–96, 2021.

[9] S. Mirsaeidi, X. Dong, D. Tzelepis, D. M. Said, A. Dyśko, and C. Booth, "A predictive control strategy for mitigation of commutation failure in lcc-based hvdc systems," *IEEE Transactions on Power Electronics*, vol. 34, no. 1, pp. 160–172, 2019.

[10] H. Xiao, X. Duan, Y. Zhang, T. Lan, and Y. Li, "Analytically quantifying the impact of strength on commutation failure in hybrid multi-infeed hvdc systems," *IEEE Transactions on Power Electronics*, vol. 37, no. 5, pp. 4962–4967, 2022.

[11] E. Rahimi, A. M. Gole, J. B. Davies, I. T. Fernando, and K. L. Kent, "Commutation failure analysis in multi-infeed hvdc systems," *IEEE Transactions on Power Delivery*, vol. 26, no. 1, pp. 378–384, 2011.

[12] B. Rehman, C. Liu, H. Li, C. Fu, and W. Wei, "Analysis on local and concurrent commutation failure of multi-infeed hvdc considering inter-converter interaction," *Journal of Modern Power Systems and Clean Energy*, vol. 10, no. 4, pp. 1050–1059, 2022.

[13] J. L. Jardim and A. M. Leite da Silva, "A methodology for computing robust dynamic equivalents of large power systems," *Electric Power Systems Research*, vol. 143, pp. 513–521, 2017.

[14] IEEE, "IEEE standard for synchrophasor data transfer for power systems," *IEEE Std C37.118.2-2011 (Revision of IEEE Std C37.118-2005)*, pp. 1–53, 2011.

[15] N. Shokouhi and J. H. L. Hansen, "Teager–kaiser energy operators for overlapped speech detection," *IEEE/ACM Transactions on Audio, Speech, and Language Processing*, vol. 25, no. 5, pp. 1035–1047, 2017.

[16] R. Ranjan, B. C. Sahana, and A. K. Bhandari, "Cardiac artifact noise removal from sleep eeg signals using hybrid denoising model," *IEEE Transactions on Instrumentation and Measurement*, vol. 71, pp. 1–10, 2022.

[17] P. Bhowmick, A. Banerjee, D. Dey, and S. Munshi, "Cross teager-kaiser energy operator based feature extraction method for gait recognition from cumulative foot pressure images," in *2018 IEEE Applied Signal Processing Conference (ASPCON)*, 2018, pp. 371–374.

[18] A.-O. Boudraa and F. Salzenstein, "Teager–kaiser energy methods for signal and image analysis: A review," *Digital Signal Processing*, vol. 78, pp. 338–375, 2018. [Online]. Available: https://www.sciencedirect.com/science/article/pii/S1051200418300927

[19] R. Yadav, A. K. Pradhan, and I. Kamwa, "Real-time multiple event detection and classification in power system using signal energy transformations," *IEEE Transactions on Industrial Informatics*, vol. 15, no. 3, pp. 1521–1531, 2019.

[20] J. Jardim and A. L. da Silva, "A methodology for computing robust dynamic equivalents of large power systems," *Electric Power Systems Research*, vol. 143, pp. 513–521, 02 2017.

[21] D. Dotta, J. Chow, and D. Bertagnolli, "A teaching tool for phasor measurement estimation," *IEEE Transactions on Power Systems*, vol. 29, pp. 1981–1988, 10 2015.

[22] "IEEE standard for synchrophasor data transfer for power systems," *IEEE Std C37.118.2-2011 (Revision of IEEE Std C37.118-2005)*, pp. 1–53, 2011.